Tertiary and quaternary allostery in HbII from *Scapharca inaequivalvis*

Luca Ronda[a], **Stefano Bettati**[b,c], **Eric R. Henry**[d], **Tara Kashav**[e], **Jeffrey M. Sanders**[e,f], **William E. Royer**[e,*], and **Andrea Mozzarelli**[a,c,*]

[a]Department of Pharmacy, University of Parma, Parco Area delle Science, 23/A, 43124 Parma, Italy

[b]Department of Neurosciences, University of Parma, Via Volturno, 39, 43125 Parma, Italy

[c]National Institute of Biostructures and Biosystems, Viale Medaglie d'Oro, 305, 00136 Rome, Italy

[d]Laboratory of Chemical Physics, National Institute of Diabetes, Digestive and Kidney Diseases, National Institutes of Health, Bethesda, MD 20892-0520, USA

[e]Department of Biochemistry and Molecular Pharmacology, University of Massachusetts Medical School, Worcester, MA 01655, USA

Abstract

The clam *Scapharca inaequivalvis* possesses two cooperative oxygen binding hemoglobins in its red cells: a homodimeric HbI and a heterotetrameric A2B2 HbII. Each AB dimeric half of HbII is assembled very similarly to that of the well studied HbI. This study presents crystal structures of HbII along with oxygen binding data both in the crystalline state and in wet nanoporous silica gels. Despite very similar ligand-linked structural transitions observed in HbI and HbII crystals, HbII in the crystal or encapsulated in silica gels apparently exhibits minimal cooperativity in oxygen binding, in contrast with the full cooperativity exhibited by HbI crystals. However, oxygen binding curves in the crystal indicate the presence of a significant functional inequivalence of A and B chains. When this inequivalence is taken into account, both crystal and R state gel functional data are consistent with the conservation of a tertiary contribution to cooperative oxygen binding, quantitatively similar to that measured for HbI, and are in keeping with the structural information. Furthermore, our results indicate that to fully express the cooperative ligand binding, HbII requires quaternary transitions hampered by crystal lattice and gel encapsulation, revealing greater complexity in cooperative function than the direct communication across a dimeric interface observed in HbI.

Keywords

X-ray crystallography; microspectrophotometry; silica gel; cooperativity; hemoglobin

[*]Corresponding Authors: Andrea Mozzarelli, Department of Pharmacy, University of Parma, Parco Area delle Scienze 23/A, 43124, Parma, Italy. andrea.mozzarelli@unipr.it. Phone: 39-0521905138. Fax: 39-0521905151. William E. Royer, Department of Biochemistry and Molecular Pharmacology, University of Massachusetts School of Medicine, 364 Plantation Street, LRB921, Worcester, MA 01605.
[f]Present address: Department of Biochemistry and Molecular Biology, Thomas Jefferson University, Philadelphia, PA 19107, USA

For over a century, the remarkable ability of hemoglobin to bind ligands cooperatively and to alter its binding properties as a function of solution environment has intrigued and perplexed investigators. Human hemoglobin A (HbA) has been the most extensively studied [1–14] but invertebrate hemoglobins, endowed with simpler or different cooperative mechanism, have provided useful alternatives to investigate cooperativity in protein function. [15, 16]

The hemoglobins of the blood clam *Scapharca inaequivalvis* are formed by three different poly-peptide chains. Two chains, designated A and B, assemble to form a heterotetramer (HbII), while a third chain assembles to form a homodimer (HbI). [17] Both HbI and HbII exhibit subunit pairing with extensive interactions between the E and F helices, a dimeric arrangement shared by all cooperative invertebrate hemoglobins with known crystal structures [16] that is entirely different from subunit pairing in the very extensively studied tetrameric mammalian hemoglobins (Figure 1). Largely due to its simplicity as a homodimer, HbI has been the most well-studied cooperative invertebrate hemoglobin. [15, 16, 18] These studies have revealed the role of tertiary interactions as the primary driving for a cooperative mechanism that involves interface water molecules and a tight coupling between contacting interface helices. [18, 19] Of particular interest is the finding that crystals of HbI exhibit full cooperative oxygen binding, indicating that the crystal lattice does not inhibit the structural transitions required for protein cooperativity. [20] Consistent with these functional results are structures of ligand transitions within crystals that show the full conformational transitions identified from earlier separate structures of liganded and unliganded HbI. [21] The full cooperative ligand binding and transitions of HbI within the crystal lattice are permitting time-resolved crystallographic experiments to identify the time-dependent structural transitions that underlie cooperativity and key intermediates that facilitate functionally important conformational changes. [18, 22, 23]

Tetrameric HbII is assembled as two heterodimers, each of which shows a very similar subunit arrangement to that of the homodimeric HbI. [24] Binding of oxygen exhibits enhanced cooperativity compared with HbI (Hill coefficient of 1.9), along with a sensitivity to pH and a ligand-linked tendency to polymerize [25], properties not observed in the homodimeric HbI.

Here, we report crystallographic and oxygen binding studies of HbII to illuminate the contribution of tertiary and quaternary structural transitions to HbII allostery. Despite similar ligand-linked structural transitions observed in HbII and HbI, only minimal levels of cooperativity are apparently expressed by crystals of HbII. Furthermore, similar oxygen binding properties are evident with HbII encapsulated in silica gels, confirming a requirement for quaternary transitions not compatible with either the crystal lattice or silica gel encapsulation. However, when oxygen binding of HbII in the crystal and encapsulated in silica gels is analyzed taking into account the large functional asymmetry of A and B subunits exhibited in the crystal and in T state gels, a tertiary contribution to cooperativity in oxygen binding appears to be maintained in R state gels and crystals of HbII. Overall, these results suggest that the allosteric properties of HbII require more complex quaternary transitions than those operating in HbI.

Materials and Methods

Chemicals

Na^+ and K^+ phosphate, EDTA and bovine liver catalase were purchased from Sigma Aldrich and are of best quality grade. Helium, oxygen, nitrogen and carbon monoxide were of research grade.

HbII purification

Purified HbII was the generous gift of Drs. Gianni Colotti and Emilia Chiancone, University of Rome.

Crystallographic analysis

HbII-CO was crystallized under high salt conditions (1.9–2.2 M Na^+/K^+ phosphate, pH 5.8) in the presence of a carbon monoxide (CO) atmosphere as described previously. [24] Crystals were mounted in cryoloops, following coating in Paratone-N and frozen in a cold-stream at BioCARS beamline 14-BMC.

Crystallization of unliganded HbII under anaerobic conditions was not successful; the propensity of unliganded HbII to polymerize [25] may have contributed to difficulties with crystallization. Instead, crystals of unliganded HbII were obtained through the ligand transition procedure previously used successfully with HbI. [21] In brief, crystals of HbII-CO were soaked in 150 mM potassium ferricyanide, 300 mM potassium cyanide, 2.2 M phosphate at pH 5.8 for two hours under a bright light to displace CO while oxidizing the heme iron. These oxidized HbII crystals were then rinsed in 2.2 M phosphate (pH 5.8) and transferred to an anaerobic chamber. Crystals were then reduced by soaking in a solution containing 150 mM sodium dithionite and 2.2 M phosphate (pH 5.8) for one to five hours before mounting. Crystals were then transferred to paratone-N, coated and mounted on a cryoloop and flash frozen in liquid nitrogen all within the anaerobic chamber. They were then shipped to BioCARS for diffraction data collection. Diffraction data revealed a cell transformation to space group $P222_1$ from the original $P2_12_12_1$ cell of HbII-CO. X-ray diffraction data (0.979 Å) were collected at BioCARS beamline BMC on an ADSC Quantum 315 detector at 100 K. Data collection statistics are shown in Table 1.

The starting point for refinement of HbII-CO was the 2 Å structure, PDB ID code 1SCT. [24] For unliganded HbII, molecular replacement with 1SCT using AMORE provided the starting point for refinement. Both structures were refined using anisotropic atomic B-factors with REFMAC5. Molecular building, including addition of alternate conformers and water molecules, was carried out with COOT. [26] Final statistics are provided in Table 1.

Accession number

Coordinates and structure factors have been deposited in the Protein Data Bank with accession number 4HRR for HbII-CO, and 4HRT for deoxy-HbII.

Oxygen binding measurements on HbII crystals

Single crystals of HbII, stored in a stabilizing solution containing 62% Na^+/K^+ phosphate, pH 5.8, equilibrated with 1 atm CO, were withdrawn from the vial and soaked in a solution with the same phosphate concentration at pH 7.0, in the presence of 4,000 U/ml bovine liver catalase. The crystals were placed in a Dvorak-Stotler flow cell [27], covered with a transparent, isotropic and oxygen permeable silicon membrane (MEM 213), and connected to a humidified gas line, as previously described. [28] The flow cell was mounted on the thermostatted stage of a Zeiss MPM03 microspectrophotometer. HbII-CO crystals were exposed to the white light of a 75 W Xenon lamp to release CO, under a flow of pure oxygen.

Polarized absorption spectra in the 450–700 nm range were collected along two of the crystal axes, as described elsewhere [28–30], as a function of oxygen partial pressure between 0 and 760 torr. Oxygen pressures were prepared by a gas mixer generator (Environics 4000 series). The fractional saturation at each oxygen partial pressure was calculated by fitting the

spectra to a linear combination of reference spectra of the pure oxy, deoxy and oxidized species. [28]

The equilibration of crystals at a defined oxygen partial pressure required from 1 to 4 hours, depending on the oxygen partial pressure. Therefore, in order to limit the amount of oxidized HbII to values less than 5%, oxygen binding curves were usually determined from data points collected on four HbII crystals.

HbII encapsulation in wet nanoporous silica gels

HbII encapsulation was carried out following the sol-gel procedure reported previously with some modifications. [30–35] A solution of tetramethyl orthosilicate (TMOS), water and hydrochloric acid was sonicated for 20 minutes. An equal volume of a solution containing 10 mM phosphate, 1 mM EDTA, pH 6.0, was added and the mixture bubbled with humidified nitrogen for 40 minutes to remove both methanol formed due TMOS hydrolysis and oxygen.

A 250 μM solution of HbII in 50 mM phosphate, 1 mM EDTA, 10 mM sodium dithionite, pH 7.2, was anaerobically mixed in 1.5:1 ratio with the sol. Gelification occurred within 10 minutes at 4 °C. HbII gels where covered with a solution containing 100 mM phosphate, 1 mM EDTA, 30 mM sodium dithionite, pH 7.0 and stored at 4 °C. R and T states were encapsulated with the same protocol, using solutions equilibrated with carbon monoxide and nitrogen, respectively.

Oxygen binding measurements on HbII in solution and encapsulated in silica gel

Oxygen binding curves on HbII in solution were carried out using a home-made tonometer [38] connected to the gas mixture generator. The samples were equilibrated for 30 minutes at different oxygen partial pressures and the spectra were collected with a Cary 400 (Varian) spectrophotometer in the 450–700 nm range. To prevent met-hemoglobin formation, the enzymatic Hayashi reduction system was added to the solution. [36]

Oxygen binding measurements on HbII gels encapsulated in either the T or R state were carried out using a Zeiss MPM03 microspectrophotometer and the same procedure followed for HbII crystals. For R state HbII gel, oxygen binding measurements were preceded by CO removal via photolysis under pure oxygen flow. In gel experiments, catalase (4,000 U/ml) was added to the buffer solution.

Solution reference spectra were collected similarly to crystals. For the determination of the oxygen fractional saturation of HbII gels, a slope function was added in the fitting procedure to account for the scattering contribution of the silica matrix to the absorption. [30, 32, 34]

Differently from human HbA gels, in which changes in oxygen affinity associated with conformational relaxations during oxygen equilibration prevent attainment of a stable fractional saturation [31], T and R HbII gel fractional saturations remain stable after the equilibration phase (10 minutes).

Gel filtration chromatography

HbII in 100 mM phosphate, 1 mM EDTA, pH 7.0, was loaded on a G-100 resin packed on a XK 16/70 column (GE Healthcare) connected to an AKTA Prime chromatographic system (GE Healthcare). Chromatographic runs were carried out at 0.2 ml/min flow rate, 20 °C. The G-100 column was calibrated using gel filtration molecular weight standard (GE Healthcare): ovalbumin (MW 43,000 Da), conalbumin (MW 75,000 Da) and horse heart myoglobin (MW 17,000 Da). To calculate the void volume, Blue Dextran 2000 was used.

Results and Discussion

Crystal structure of HbII-CO

The resolution of the crystal structure of carbon monoxide bound HbII has been extended from the earlier published 2.0 Å structure [24] to 1.25 Å, as a result of data collection on frozen crystals at BioCARS beamline 14-BMC. The asymmetric unit of these crystals is formed from two HbII tetramers, including four A chains and four B chains. Crystallographic statistics of the analysis are provided in Table 1.

HbII is assembled as two AB heterodimers related by a molecular dyad as shown in Figure 1b. Each AB heterodimer is assembled nearly identically to the HbI homodimer (Figure 1c) with extensive interactions between the E and F helices. The key interface residues in the HbI homodimer are maintained in the HbII AB dimers. At the periphery of the interface, however, a few differences are evident, as discussed in our earlier analysis of HbI-CO. [24]

The higher resolution crystallographic analysis of HbII-CO presented here confirms many of the structural features described for the crystal structure at 2.0 Å resolution. [24] However one striking finding not detected earlier is that Phe F4 apparently adopts alternate conformations in two of the four A subunits in HbII-CO crystals. (Residues are identified by their helical notation using the standard globin designation. Phe F4, which is residue 97 in A subunits and residue 99 in B subunits, is homologous to the fourth residue in the F helix of sperm whale myoglobin, and is thus designated as F4 even though it is the 12th residue in the longer F-helix found in HbII and other invertebrate hemoglobins). In HbI, Phe F4 packs in the heme pocket in the unliganded form, characteristic of the low affinity "T" state, but is extruded into the subunit interface when either CO or O_2 is bound to form the high affinity "R" state. [37, 38] Mutagenesis has confirmed a central role for Phe F4 in regulating oxygen affinity [39], which appears to derive largely from a steric effect of packing into the heme pocket in the unliganded form to restrict movement of the heme iron into the heme plane required for acquisition of a high affinity conformation. Given its central role in regulating oxygen affinity in HbI, the observation of clear density (Figure 2) indicating a mixture of T and R signatures in two of the four A subunits was surprising. In contrast, Phe F4 shows the expected R-state conformation placing its side chain in the dimeric interface in all B subunits, and in two of the A subunits, with no evidence of packing in the T-state position (Figure 2). Thus, the HbII-CO crystals exhibit evidence of some T-state structural properties, but most subunits exhibit expected R-state structures.

Crystal structure of unliganded HbII

We obtained a structure of unliganded HbII by transforming the ligand state within crystals grown in the HbII-CO state. This was done by removing the CO ligands by oxidizing the heme iron and then reducing it under anerobic conditions, as was successful in earlier experiments with HbI. [21]

Comparisons of the CO-liganded and unliganded structures of HbII reveal transitions within each AB dimer that are very similar to those observed in the dimeric HbI. All subunits in the unliganded HbII structure exhibit the expected T-state conformations, including Phe F4 that exhibited both T and R-state conformations in two subunits of HbII-CO (Figure 2). A particularly notable aspect of the ligand-linked structural transitions in HbI is a dramatic rearrangement of interface water molecules that has been demonstrated to play a central role in oxygen affinity and intersubunit communication. [19] Ligand binding in HbII is coupled with a very similar rearrangement of interface water molecules (Figure 3). As in HbI, there is a core of five very well ordered water molecules (dark blue, in Figure 3) that is maintained in both liganded and unliganded HbII AB dimers. Ligand binding, accompanied by an extrusion of Phe F4 into the dimeric interface, results in a striking rearrangement of

very well ordered water molecules (light blue in Figure 3). The very well ordered interface water molecules in unliganded HbII dimers are essentially identical to those of HbI, whereas the less well ordered interface water molecules in HbII-CO dimers are similar, but not identical, to those of HbI.

Ligand binding is coupled with rotations between EF dimer subunits that are slightly larger than those observed with HbI. In HbI, ligand binding results in subunits rotating relative to each other by 3.4°. Comparisons of the four dimers per asymmetric unit in HbII and HbII-CO reveal that ligand release results in rotations between the EF dimer pairs that range from 3.8° to 5.1°, with ligand-linked subunit rotations in the same direction as those for HbI. Thus, the crystal lattice does not prevent subunit rotations that are sufficient for full cooperativity in the HbI EF dimer. Somewhat larger interdimer rotations are observed, with ligand release resulting in rotations of the dimer arrangement in the two crystallographically unique tetramers of 5.1° and 6.2°. The overall motion of subunits is complex; unlike human hemoglobin no pair of subunits moves together, rather all subunits rotate relative to each other by at least 3.8°. As can be seen in Figure 4, ligand-linked rotations are in similar, but not identical, directions for the subunits within the HbII tetramer.

Oxygen binding to HbII in solution

Oxygen binding curves for HbII in solution were determined and fitted to the Hill equation (Figure 5, dashed line), yielding a p50 of 7.73 ± 0.12 torr and a Hill coefficient of 1.90 ± 0.05. The affinity for binding of the first $(1/K_1)$ and the fourth $(1/K_4)$ oxygen molecule to HbII, as calculated by analyzing the oxygen binding curve with the Adair equation (Figure 5, solid line) is 22.4 ± 3.7 and 1.33 ± 0.61 torr, respectively. Oxygen binding curves measured at heme concentrations ranging from 3.4 to 107 μM were found to be fully superimposable (data not shown). To further verify whether HbII in solution is present in a pure tetrameric form at the concentrations used for this work, gel filtration experiments were carried out at 5.6 and 107 μM HbII, loading a volume of 0.5 ml of protein on a G-100 Sephadex column. For comparison, HbA at similar concentrations was loaded on the column. From the elution volumes of HbA and HbII (Figure 6), the estimated molecular weights are 45,300 and 30,400 Da for HbA at 100 and 2 μM, respectively, and 60,100 Da for HbII at 107 and 5.6 μM. These results point out that the HbII tetramer in solution is more stable than HbA, and, in the liganded state, HbII tetramer polymerization does not occur. Indeed, HbII polymerization occurs at higher concentration. [17]

Oxygen binding to HbII crystals

For the evaluation of the oxygen fractional saturation of HbII crystals, reference spectra for oxy-, deoxy-, and met-hemoglobin were determined. [28] A single HbII crystal, stored in 1 atm CO, was photolyzed under pure oxygen flow to obtain the pure oxygenated species. Polarized absorption spectra were collected with light linearly polarized along the *c* and *a* crystal axis, respectively (Figure 7). The crystal was then washed with a deoxygenated solution in the presence of 30 mM sodium dithionite to obtain the pure deoxygenat-ed species and the corresponding polarized spectra were recorded (Figure 7). Finally, the crystal was soaked in a solution containing 5 mM potassium ferricyanide to generate the pure met-hemoglobin species (Figure 7). The polarization ratio, i.e. the ratio of the absorbance along the two axes as a function of wavelength is reported in Figure 7a.

HbII-CO crystals were soaked in an air-equilibrated solution, loaded on the Dvorak-Stotler flow cell and mounted on the microspectrophotomer stage. After CO photolysis under 1 atm oxygen flow, the crystals were exposed to defined oxygen pressures. To ascertain full reversibility of oxygen binding, polarized absorption spectra were recorded as a function of either decreasing or increasing oxygen pressures (Figure 8). Observed spectra were fitted to

a linear combination of reference spectra to calculate the fractional saturation of oxygenated hemes. HbII crystals showed a Hill coefficient of 1.05 ± 0.07 and 1.14 ± 0.06 for binding curves measured with light polarized parallel to the *c* and *a* crystal axes, respectively (Figure 8). This value is significantly lower than the value measured in solution under similar experimental conditions (Hill coefficient of 1.90 ± 0.05), suggesting that homotropic allostery is severely hampered by the crystal lattice. This finding is different from that previously observed for crystals of HbI from *Scapharca inaequivalvis*, where the cooperativity was essentially the same in the crystal (Hill coefficient of 1.43 ± 0.07 and 1.46 ± 0.06 for data recorded along the *a* and *b* axis, respectively) and in solution (1.44). [20] Although the dimeric HbI and the AB dimer of HbII share similar contacts and assembly, it seems that the quaternary transition involving the interdimer rearrangements plays a fundamental role in controlling cooperativity of HbII oxygen binding, despite the previous observation that tertiary mechanisms are responsible for HbI cooperativity. [20, 21, 38] However, the structural information reported above suggests that a tertiary contribution to HbII homotropic cooperativity, with a similar mechanism to HbI, could be at work. This apparent discrepancy seems to be solved by carefully analyzing oxygen binding data in the crystals. Indeed, the values of p50s measured along the two polarization directions are significantly different, 2.57 ± 0.18 and 1.57 ± 0.10 torr for the oxygen binding curves measured with light polarized parallel to the *c* and *a* crystal axes, respectively (Figure 8). This difference is observed despite that the overall projections of the four A hemes present in the unit cells are very close to those of the B hemes (Table 2). [28, 40, 41] This finding indicates that the oxygen affinity inequivalence between A and B chains within the HbII dimer must be quantitatively relevant. High oxygen affinity inequivalence between A and B hemes is necessarily associated with a Hill coefficient value lower than 1, that leads to an underestimation of the actual positive cooperativity of HbII in the crystal. Furthermore, the observed p50s of HbII in the crystal are lower than the p50 in solution (7.73 ± 0.12 torr), and about two-fold higher than the oxygen affinity for the binding of the fourth oxygen, $1/K_4 = 1.33 \pm 0.61$ torr (see Figure 5). This result indicates that the crystal lattice stabilizes a high affinity conformation of HbII.

Oxygen binding to HbII encapsulated in silica gels

Encapsulation of HbA in wet, nanoporous silica gels was demonstrated to slow down by several orders of magnitude the conformational transitions associated to ligand binding. [8, 30–32, 34, 42–45] Therefore, encapsulation allows characterization of distinct quaternary/tertiary states that are not normally accessible to spectroscopic investigation in solution.

HbII was encapsulated in silica gels under either deoxy or oxy conditions (see Materials and Methods). Oxygen binding curves were measured for either deoxy-HbII (T state) or oxy-HbII gels (R state), under the same experimental conditions used for solution experiments, collecting absorption spectra as a function of increasing or decreasing oxygen pressures.

For R state HbII gels the Hill coefficient is 1.06 ± 0.02 (Figure 9), very similar to the Hill coefficient observed in the crystal. The p50 is 3.4 ± 0.1 torr, higher than that found in R state crystals. This difference might be due to an effect of the high ionic strength present in the crystal stabilizing solution containing 2.55 M phosphate. To confirm this effect, an R state HbII gel was soaked in a solution containing an increasing concentration of phosphate, spanning from 100 to 600 mM, 1 mM EDTA, pH 7. The samples were equilibrated at an oxygen pressure of 3.40 torr, at 15 °C. The fractional saturation was found to increase with phosphate concentration (Figure 9). At the higher phosphate concentration, the p50 of R state HbII gels was estimated to be 2.07 torr, very close to the p50 of R state HbII crystals and to $1/K_4$ of HbII in solution.

For T state gels, the oxygen binding curve exhibits a p50 of 25.6 ± 0.9 torr (Figure 9). This value is very close to the oxygen affinity determined in solution for the binding of the first oxygen, $1/K_1 = 22.4 \pm 3.7$ torr (Figure 5, solid line). This finding indicates that the encapsulation in silica gels has locked deoxy-HbII in the T state conformation, as previously observed for HbA. [8, 31, 32, 42] The calculated Hill coefficient is 0.85 ± 0.02. This value, lower than unity, is likely due to the A and B hemes inequivalence, which leads to an apparent negative cooperativity. The fact that the Hill coefficient value is even lower than that found in R state HbII crystals and gels might be due to an A/B inequivalence in the T state that is higher than that in the R state, or to further sources of functional heterogeneity originating from a distribution of tertiary states/substates. However, for HbA, $1/K_1$ is similar to the p50 measured for both deoxyHb crystals and T state Hb gels in the presence of saturating concentrations of negative allosteric effectors [8, 29, 32, 41] indicating that gel encapsulation under deoxy conditions locks Hb in the most "tense" T structure. The same effect likely occurs in HbII where encapsulation seems to abolish the contribution of both the tertiary and quaternary relaxations to homotropic cooperativity.

Estimate of tertiary cooperativity in HbII crystals

The Hill coefficient lower than one for T state HbII gels (Hill n = 0.87) suggests the presence of functionally heterogeneous subunits. The fitting of oxygen binding curves of T state HbII gels to the sum of two binding hyperbola for equally populated non-cooperative sites (Figure 10a) led to the determination of an oxygen affinity ratio of 4.9 between the two sites. When the fractional saturation as a function of oxygen pressure for R-state HbII gels (Figure 10b) was fitted to two binding hyperbola with equally populated binding sites, a binding cooperativity fixed to the same value measured for HbI in solution and in the crystalline state (Hill coefficient of 1.44) [20], and an oxygen affinity ratio fixed to 4.9, the value derived from T state HbII gels, the calculated p50 was found to be 1.64 torr for the higher affinity site, very close to the value measured for $1/K_4$ in solutions, 1.33 torr. The goodness of the fit clearly indicates that a significant contribution to homotropic cooperativity arises from tertiary relaxations that are allowed in R-state HbII gels. Tertiary cooperativity appears to be partially masked by the functional asymmetry of A and B chains. On the other side, crystallization and encapsulation in silica gel prevent the R-to-T quaternary conformational change which is responsible for the remaining, large part of HbII homotropic cooperativity (overall Hill coefficient of 1.9 in solution).

Individual oxygen binding curves for the A and B subunits of HbII in the crystal could be extracted from the binding curves measured with light polarized parallel to two different crystal axes (Figure 8) and the known projections of all hemes along the same axes (Table 2), following the formalism reported previously. [28] However, such analysis is very sensitive to small differences in heme geometry and in the projection of heme normal along the crystal axes. This, together with averaging arising from the presence of two tetramers per unit cell, makes it very difficult to achieve an accurate estimate of the oxygen affinity of A and B hemes in R-state HbII crystals. Nevertheless, as stated above, the large separation of the p50s measured along two crystal axes indicates that A and B chains must be endowed with markedly different oxygen affinities. The functional asymmetry of subunits in HbII can be investigated exploiting approaches previously carried out for human HbA, such as laser-photolysis techniques[46, 47] or kinetic and equilibrium experiments on metal hybrid Hbs in which one pair of subunits has an inert metal-porphyrin group. [48–50]

Conclusions

The pioneering work carried out by Shibayama and coworkers exploiting the sol-gel method to fix quaternary states [42] was later expanded by other groups, with the aim of investigating the relationship between tertiary and quaternary states in the control of functional properties

of tetrameric hemoglobin. In particular, the key observation arising from the work of Mozzarelli, Friedman, Shibayama, Spiro and their groups was that i) functionally and structurally distinct tertiary conformations exist within a single quaternary state [8, 31, 32, 34, 51–54], and ii) cooperativity is suppressed in the absence of quaternary relaxations. [8, 31, 32, 53]

The experiments presented here clearly demonstrate that quaternary transitions, not compatible with the crystal lattice or with encapsulation in silica gels, are required for the full expression of oxygen binding cooperativity in HbII. An unexpected result is that oxygen binding curves to R-state gels and crystal, despite the assembly of non identical subunits into the HbII tetramer, are consistent with the quantitative conservation of a tertiary mechanism of intra-dimer cooperativity similar to that observed for homodimeric HbI. This is in full agreement with the structural information derived in the present work, given the similarity in the structure and ligand-linked structural transitions of HbII compared with HbI.

Acknowledgments

ABBREVIATIONS

HbA   human hemoglobin A

HbII   tetrameric HbII from *Scapharca inaequivalis*

**HbI**   dimeric HbI from *Scapharca inaequivalis.*

References

1. Eaton WA, Henry ER, Hofrichter J, Bettati S, Viappiani C, Mozzarelli A. Evolution of allosteric models for hemoglobin. IUBMB Life. 2007; 59:586–599. [PubMed: 17701554]

2. Henry ER, Bettati S, Hofrichter J, Eaton WA. A tertiary two-state allosteric model for hemoglobin. Biophys Chem. 2002; 98:149–164. [PubMed: 12128196]

3. Pauling L. The oxygen equilibrium of hemoglobin and its structural interpretation. Proc Natl Acad Sci USA. 1935; 21:186–191. [PubMed: 16587956]

4. Perutz MF, Fermi G, Luisi B, Shaanan B, Liddington RC. Stereochemistry of cooperative mechanisms in hemoglobin. Cold Spring Harb Symp Quant Biol. 1987; 52:555–565. [PubMed: 3454276]

5. Yonetani T, Laberge M. Protein dynamics explain the allosteric behaviors of hemoglobin. Biochim Biophys Acta. 2008; 1784:1146–1158. [PubMed: 18519045]

6. Szabo A, Karplus M. Analysis of cooperativity in hemoglobin. Valency hybrids, oxidation, and methemoglobin replacement reactions. Biochemistry. 1975; 14:931–940. [PubMed: 235946]

7. Antonini, E.; Brunori, M. Hemoglobin and Myoglobin in Their Reactions with Ligands. Vol. 21. North-Holland: Amsterdam-London; 1971.

8. Viappiani C, Bettati S, Bruno S, Ronda L, Abbruzzetti S, Mozzarelli A, Eaton WA. New insights into allosteric mechanisms from trapping unstable protein conformations in silica gels. Proc Natl Acad Sci USA. 2004; 101:14414–14419. [PubMed: 15385676]

9. Jones EM, Balakrishnan G, Spiro TG. Heme reactivity is uncoupled from quaternary structure in gel-encapsulated hemoglobin: A resonance Raman spectroscopic study. J Am Chem Soc. 2012; 134:3461–3471. [PubMed: 22263778]

10. Eaton WA, Henry ER, Hofrichter J, Mozzarelli A. Is cooperative oxygen binding by hemoglobin really understood? Nat Struct Biol. 1999; 6:351–358. [PubMed: 10201404]

11. Ackers GK, Holt JM. Asymmetric cooperativity in a symmetric tetramer: Human hemoglobin. J Biol Chem. 2006; 281:11441–11443. [PubMed: 16423822]

12. Mills FC, Ackers GK. Quaternary enhancement in binding of oxygen by human hemoglobin. Proc Natl Acad Sci USA. 1979; 76:273–277. [PubMed: 284341]

13. Silva MM, Rogers PH, Arnone A. A third quaternary structure of human hemoglobin A at 1.7-Å resolution. J Biol Chem. 1992; 267:17248–17256. [PubMed: 1512262]

14. Smith FR, Lattman EE, Carter CW Jr. The mutation beta 99 Asp-Tyr stabilizes Y- a new, composite quaternary state of human hemoglobin. Proteins. 1991; 10:81–91. [PubMed: 1896430]

15. Royer WE Jr, Knapp JE, Strand K, Heaslet HA. Cooperative hemoglobins: Conserved fold, diverse quaternary assemblies and allosteric mechanisms. Trends Biochem Sci. 2001; 26:297–304. [PubMed: 11343922]

16. Royer WE Jr, Zhu H, Gorr TA, Flores JF, Knapp JE. Allosteric hemoglobin assembly: Diversity and similarity. J Biol Chem. 2005; 280:27477–27480. [PubMed: 15932877]

17. Chiancone E, Vecchini P, Verzili D, Ascoli F, Antonini E. Dimeric and tetrameric hemoglobins from the mollusc *Scapharca inaequivalvis* Structural and functional properties. J Mol Biol. 1981; 152:577–592. [PubMed: 7328663]

18. Ren Z, Srajer V, Knapp JE, Royer WE Jr. Cooperative macromolecular device revealed by meta-analysis of static and time-resolved structures. Proc Natl Acad Sci USA. 2012; 109:107–112. [PubMed: 22171006]

19. Royer WE Jr, Pardanani A, Gibson QH, Peterson ES, Friedman JM. Ordered water molecules as key allosteric mediators in a cooperative dimeric hemoglobin. Proc Natl Acad Sci USA. 1996; 93:14526–14531. [PubMed: 8962085]

20. Mozzarelli A, Bettati S, Rivetti C, Rossi GL, Colotti G, Chiancone E. Cooperative oxygen binding to *Scapharca inaequivalvis* hemoglobin in the crystal. J Biol Chem. 1996; 271:3627–3632. [PubMed: 8631972]

21. Knapp JE, Royer WE Jr. Ligand-linked structural transitions in crystals of a cooperative dimeric hemoglobin. Biochemistry. 2003; 42:4640–4647. [PubMed: 12705827]

22. Knapp JE, Pahl R, Cohen J, Nichols JC, Schulten K, Gibson QH, Srajer V, Royer WE Jr. Ligand migration and cavities within *Scapharca* dimeric HbI: Studies by time-resolved crystallography, Xe binding and computational analysis. Structure. 2009; 17:1494–1505. [PubMed: 19913484]

23. Knapp JE, Pahl R, Srajer V, Royer WE Jr. Allosteric action in real time: Time-resolved crystallographic studies of a cooperative dimeric hemoglobin. Proc Natl Acad Sci USA. 2006; 103:7649–7654. [PubMed: 16684887]

24. Royer WE Jr, Heard KS, Harrington DJ, Chiancone E. The 2.0 Å crystal structure of *Scapharca* tetrameric hemoglobin: Cooperative dimers within an allosteric tetramer. J Mol Biol. 1995; 253:168–186. [PubMed: 7473710]

25. Boffi A, Vecchini P, Chiancone E. Anion-linked polymerization of the tetrameric hemoglobin from *Scapharca inaequivalvis* Characterization and functional relevance. J Biol Chem. 1990; 265:6203–6209. [PubMed: 2156844]

26. Emsley P, Cowtan K. Coot: Model-building tools for molecular graphics. Acta Crystallogr D Biol Crystallogr. 2004; 60:2126–2132. [PubMed: 15572765]

27. Dvorak JA, Stotler WF. A controlled-environment culture system for high resolution light microscopy. Exp Cell Res. 1971; 68:144–148. [PubMed: 4939849]

28. Rivetti C, Mozzarelli A, Rossi GL, Henry ER, Eaton WA. Oxygen binding by single crystals of hemoglobin. Biochemistry. 1993; 32:2888–2906. [PubMed: 8457555]

29. Mozzarelli A, Rivetti C, Rossi GL, Henry ER, Eaton WA. Crystals of haemoglobin with the T quaternary structure bind oxygen noncooperatively with no Bohr effect. Nature. 1991; 351:416–419. [PubMed: 2034292]

30. Ronda L, Bruno S, Faggiano S, Bettati S, Mozzarelli A. Oxygen binding to heme proteins in solution, encapsulated in silica gels, and in the crystalline state. Methods Enzymol. 2008; 437:311–328. [PubMed: 18433635]

31. Bettati S, Mozzarelli A. T state hemoglobin binds oxygen noncooperatively with allosteric effects of protons, inositol hexaphosphate, and chloride. J Biol Chem. 1997; 272:32050–32055. [PubMed: 9405399]

32. Bruno S, Bonaccio M, Bettati S, Rivetti C, Viappiani C, Abbruzzetti S, Mozzarelli A. High and low oxygen affinity conformations of T state hemoglobin. Protein Sci. 2001; 10:2401–2407. [PubMed: 11604545]

33. Ronda L, Abbruzzetti S, Bruno S, Bettati S, Mozzarelli A, Viappiani C. Ligand-induced tertiary relaxations during the T-to-R quaternary transition in hemoglobin. J Phys Chem B. 2008; 112:12790–12794. [PubMed: 18783270]

34. Ronda L, Bruno S, Viappiani C, Abbruzzetti S, Mozzarelli A, Lowe KC, Bettati S. Circular dichroism spectroscopy of tertiary and quaternary conformations of human hemoglobin entrapped in wet silica gels. Protein Sci. 2006; 15:1961–1967. [PubMed: 16823042]

35. Ronda L, Faggiano S, Bettati S, Hellmann N, Decker H, Weidenbach T, Mozzarelli A. Hemocyanin from *E. californicum* encapsulated in silica gels: Oxygen binding and conformational states. Gene. 2007; 398:202–207. [PubMed: 17512140]

36. Hayashi A, Suzuki T, Shin M. An enzymic reduction system for metmyoglobin and methemoglobin, and its application to functional studies of oxygen carriers. Biochim Biophys Acta. 1973; 310:309–316. [PubMed: 4146292]

37. Condon PJ, Royer WE Jr. Crystal structure of oxygenated *Scapharca* dimeric hemoglobin at 1.7-Å resolution. J Biol Chem. 1994; 269:25259–25267. [PubMed: 7929217]

38. Royer WE Jr. High-resolution crystallographic analysis of a co-operative dimeric hemoglobin. J Mol Biol. 1994; 235:657–681. [PubMed: 8289287]

39. Knapp JE, Bonham MA, Gibson QH, Nichols JC, Royer WE Jr. Residue F4 plays a key role in modulating oxygen affinity and cooperativity in *Scapharca* dimeric hemoglobin. Biochemistry. 2005; 44:14419–14430. [PubMed: 16262242]

40. Kavanaugh JS, Chafin DR, Arnone A, Mozzarelli A, Rivetti C, Rossi GL, Kwiatkowski LD, Noble RW. Structure and oxygen-affinity of crystalline DesArg141-alpha human hemoglobin A in the T-state. J Mol Biol. 1995; 248:136–150. [PubMed: 7731039]

41. Mozzarelli A, Rivetti C, Rossi GL, Eaton WA, Henry ER. Allosteric effectors do not alter the oxygen affinity of hemoglobin crystals. Protein Sci. 1997; 6:484–489. [PubMed: 9041656]

42. Shibayama N, Saigo S. Fixation of the quaternary structures of human adult haemoglobin by encapsulation in transparent porous silica gels. J Mol Biol. 1995; 251:203–209. [PubMed: 7643396]

43. Shibayama N. Functional analysis of hemoglobin molecules locked in doubly liganded conformations. J Mol Biol. 1999; 285:1383–1388. [PubMed: 9917383]

44. Abbruzzetti S, Viappiani C, Bruno S, Bettati S, Bonaccio M, Mozzarelli A. Functional characterization of heme proteins encapsulated in wet nanoporous silica gels. J Nanosci Nanotechnol. 2001; 1:407–415. [PubMed: 12914082]

45. Bruno S, Ronda L, Bettati S, Mozzarelli A. Trapping hemoglobin in rigid matrices: Fine tuning of oxygen binding properties by modulation of encapsulation protocols. Artif Cells Blood Substit Immobil Biotechnol. 2007; 35:69–79. [PubMed: 17364472]

46. Lepeshkevich SV, Parkhats MV, Stepuro II, Dzhagarov BM. Molecular oxygen binding with alpha and beta subunits within the R quaternary state of human hemoglobin in solutions and porous sol-gel matrices. Biochim Biophys Acta. 2009; 1794:1823–1830. [PubMed: 19716936]

47. Philo JS, Lary JW. Kinetic investigations of the quaternary enhancement effect and alpha/beta differences in binding the last oxygen to hemoglobin tetramers and dimers. J Biol Chem. 1990; 265:139–143. [PubMed: 2294099]

48. Bettati S, Mozzarelli A, Rossi GL, Tsuneshige A, Yonetani T, Eaton WA, Henry ER. Oxygen binding by single crystals of hemoglobin: The problem of cooperativity and inequivalence of alpha and beta subunits. Proteins-Struct Funct Genet. 1996; 25:425–437. [PubMed: 8865338]

49. Bruno S, Bettati S, Manfredini M, Mozzarelli A, Bolognesi M, Deriu D, Rosano C, Tsuneshige A, Yonetani T, Henry ER. Oxygen binding by alpha(Fe^{2+})(2)beta(Ni^{2+})(2) hemoglobin crystals. Protein Sci. 2000; 9:683–692. [PubMed: 10794410]

50. Unzai S, Eich R, Shibayama N, Olson JS, Morimoto H. Rate constants for O-2 and CO binding to the alpha and beta subunits within the R and T states of human hemoglobin. J Biol Chem. 1998; 273:23150–23159. [PubMed: 9722544]

51. Samuni U, Dantsker D, Juszczak LJ, Bettati S, Ronda L, Mozzarelli A, Friedman JM. Spectroscopic and functional characterization of T state hemoglobin conformations encapsulated in silica gels. Biochemistry. 2004; 43:13674–13682. [PubMed: 15504030]

52. Samuni U, Roche CJ, Dantsker D, Juszczak LJ, Friedman JM. Modulation of reactivity and conformation within the T-quaternary state of human hemoglobin: The combined use of mutagenesis and sol-gel encapsulation. Biochemistry. 2006; 45:2820–2835. [PubMed: 16503637]

53. Shibayama N, Saigo S. Direct observation of two distinct affinity conformations in the T state human deoxyhemoglobin. FEBS Lett. 2001; 492:50–53. [PubMed: 11248235]

54. Jones EM, Balakrishnan G, Spiro TG. Heme reactivity is uncoupled from quaternary structure in gel-encapsulated hemoglobin: A resonance Raman spectroscopic study. J Am Chem Soc. 2012; 134:3461–3471. [PubMed: 22263778]
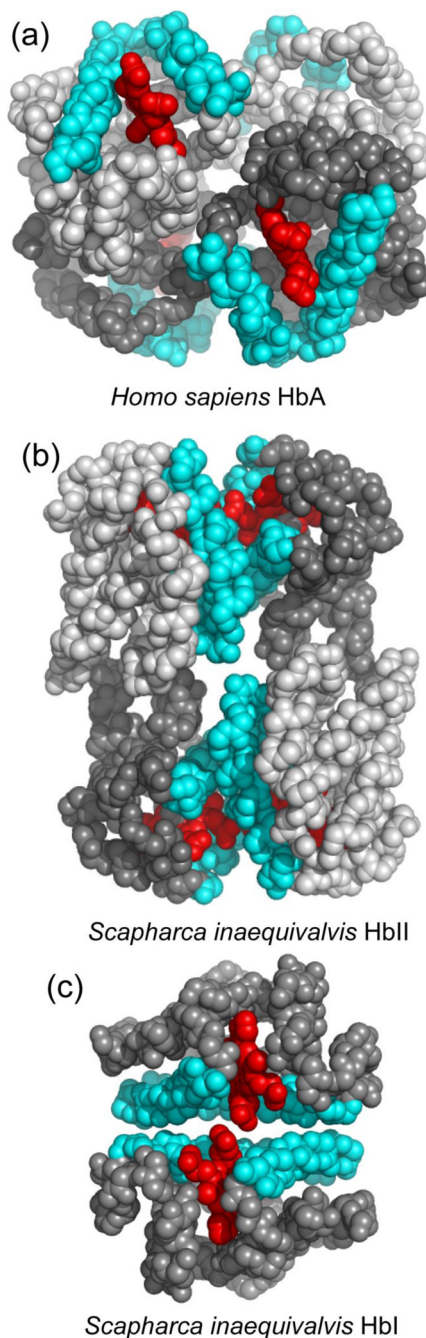
Figure 1.
Quaternary assembly of human and clam hemoglobins. Subunits are depicted as van der Waals spheres for main chain and heme atoms, with heme groups shown in red, E and F helices in cyan and the rest of the main chain in gray. (a) Human oxygenated HbA (PDB code 1HHO) is shown with α subunits in dark gray and β subunits in light gray. Note how the E and F helices are on the outside of the molecule. (b) *Scapharca inaequivalvis* tetrameric HbII-CO (PDB code 1SCT) is shown viewed approximately along its molecular dyad with A subunits in dark gray and B subunits in light gray. Note the extensive subunit pairings involving the E and F helices. (c) *Scapharca inaequivalvis* homodimeric HbI-CO

(PDB code 3SDH) viewed approximately along its molecular dyad showing the extensive dimeric interactions involving the E and F helices.
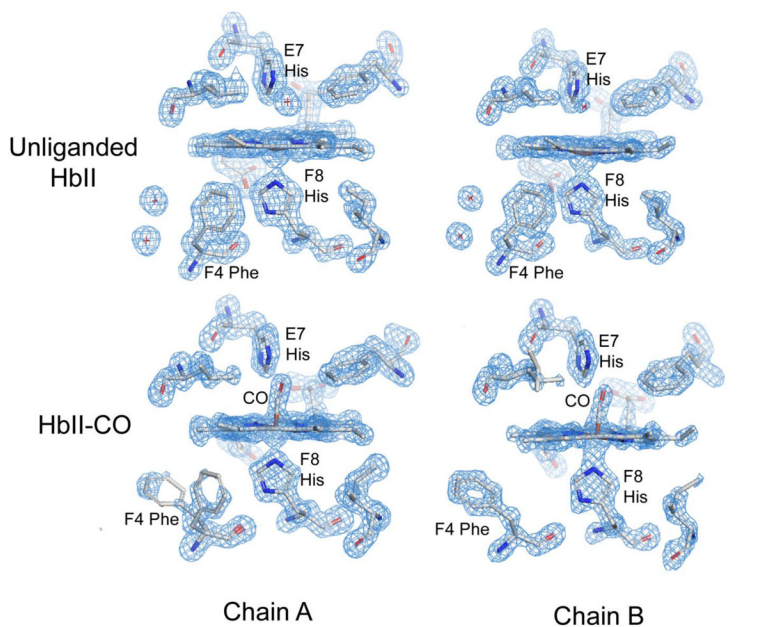
Figure 2.
Fo–Fc omit maps, contoured at 3 σ, for the heme region of two of the subunits in both unliganded and CO-liganded form. The top two figures show the unliganded heme region with expected structural features, based on earlier analyses of the homodimeric HbI. In all eight subunits, Phe F4 packs in the heme pocket contacting both heme and proximal histidine atoms characteristic of the low affinity "T" state. As well, density is clearly evident in the figure for two of the T-state specific interface water molecules. The lower two figures show the CO-liganded forms of one A and one B subunit. The density for Phe F4 in the CO ligated form for the chain A shown indicates the presence of two alternate conformations for this residue. In this subunit, and one other A-type subunit, both T-state and R-state conformations of Phe F4 are present. In the other two A-type subunits and all four B-type subunits, the side-chain of Phe F4 packs in the subunit interface as evident in the lower right figure and is characteristic of the high affinity R-state form of the homodimeric HbI.
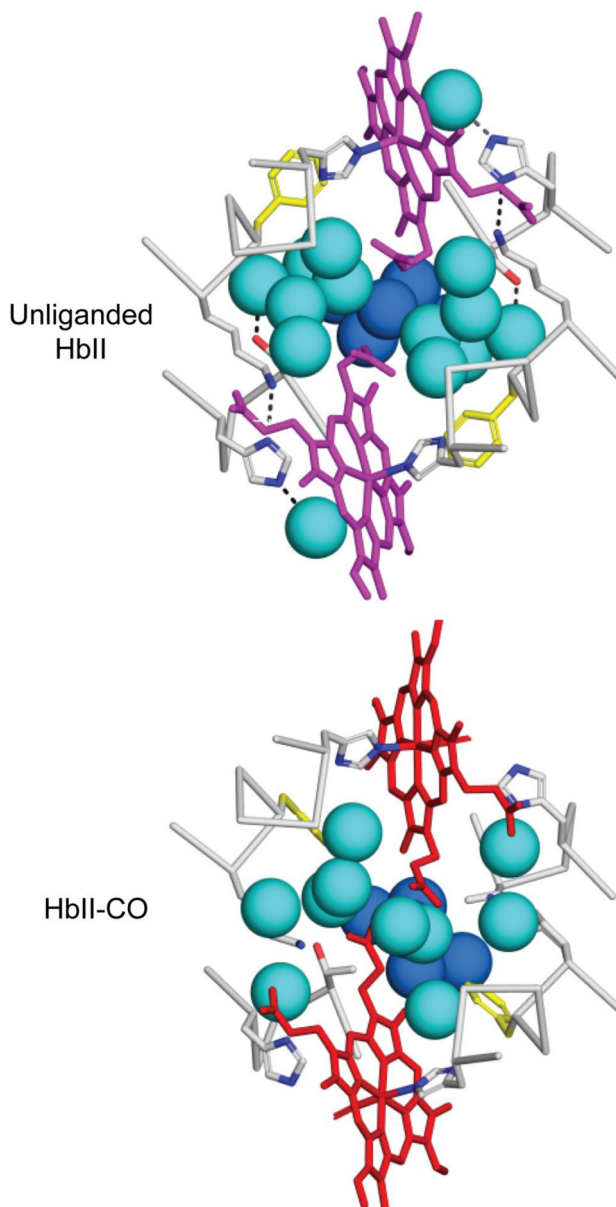
Figure 3.
Ligand-linked transitions of core interface water molecules in HbII. The images show portions of the E and F helices and heme groups along with spheres for key water molecules. Five water molecules that are unaltered by ligation are shown as dark blue, with the remaining water molecules as light blue/cyan. The arrangement of water molecules and side chains shown at the top for unliganded HbII is indistinguishable from the conformations observed in unliganded HbI. The water arrangement for HbII-CO is similar to that for HbI-CO, but not identical, showing additional water molecules and some variability among AB dimers. The water structure, along with the variation of Phe F4 in HbII-CO suggests that in these crystals HbII-CO does not obtain as pure an R-state structure as has been earlier observed with both oxygenated and CO-liganded HbI.
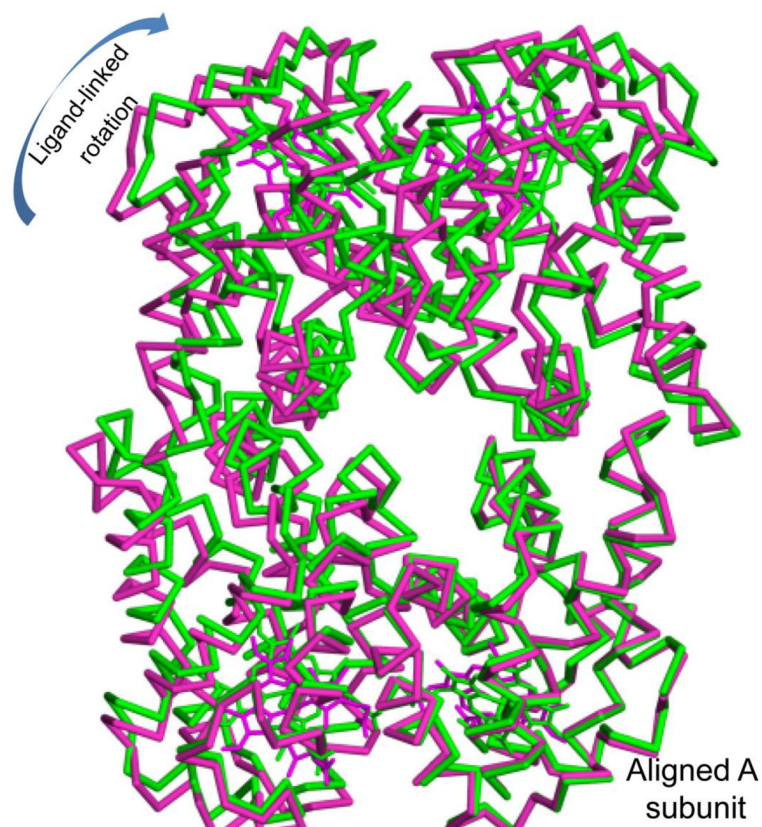
Figure 4.
Alpha-carbon trace for HbII-CO (green) and unliganded HbII (purple) following alignment
of one A chain (lower right). As can be seen, ligand binding results in rotations of all
subunits, in a generally clockwise direction for the view shown. Subunit rotations illustrated
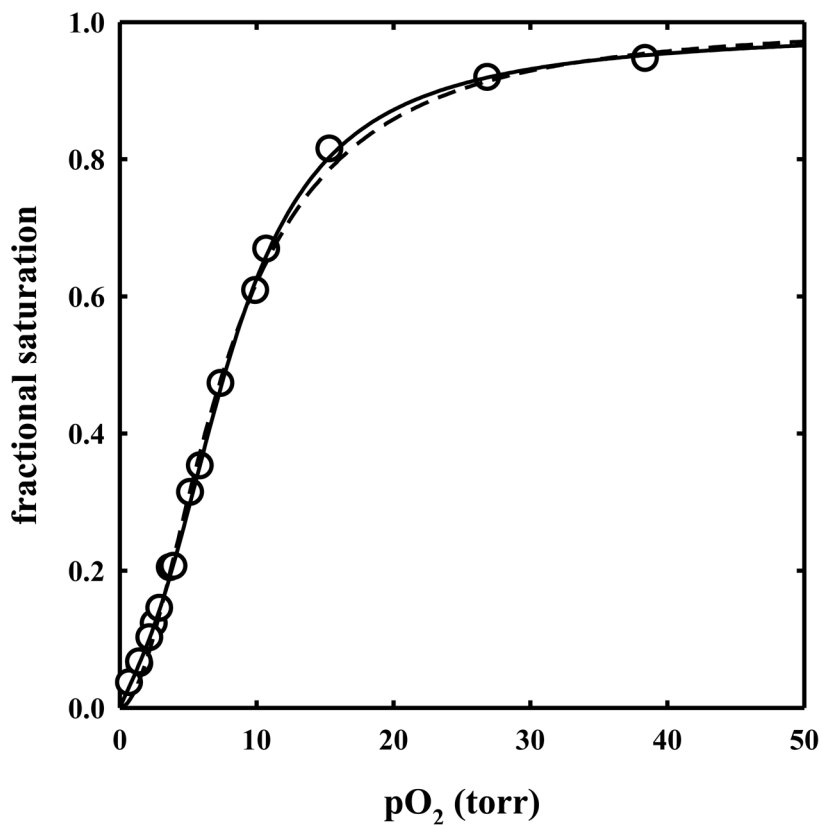here range from 3.8–6.5°.

Figure 5.
Oxygen binding curve to HbII in a solution containing 100 mM phosphate, 1 mM EDTA, pH 7.0, 15 °C (open circles). Data points were fitted to the Hill equation (dashed line) with a p50 of 7.73 ± 0.12 torr and a Hill coefficient of 1.90 ± 0.05, and to the Adair equation (solid line) with dissociation constants: $K_1 = 0.0446 \pm 0.0072$ torr^{-1}, $K_2 = 0.0502 \pm 0.0268$ torr^{-1}, $K_3 = 0.1974 \pm 0.1319$ torr^{-1}, $K_4 = 0.7524 \pm 0.2348$ torr^{-1}.
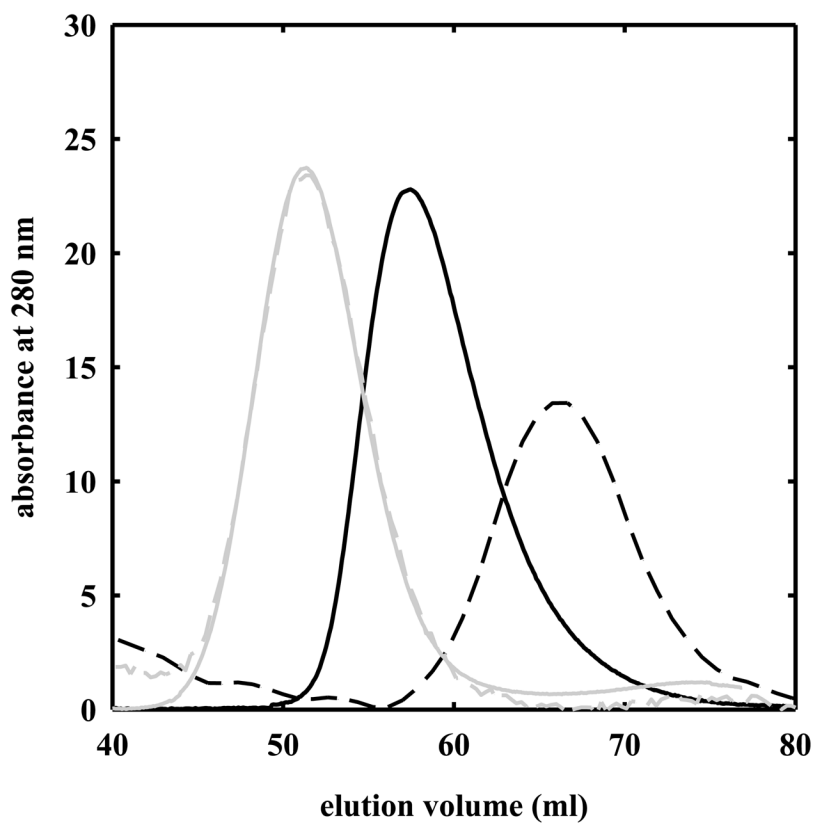
Figure 6.
Elution profiles of G-100 Sephadex size exclusion chromatography of solutions containing
100 µM (solid black line) and 2 µM HbA (dashed black line), and 107 µM (solid grey line)
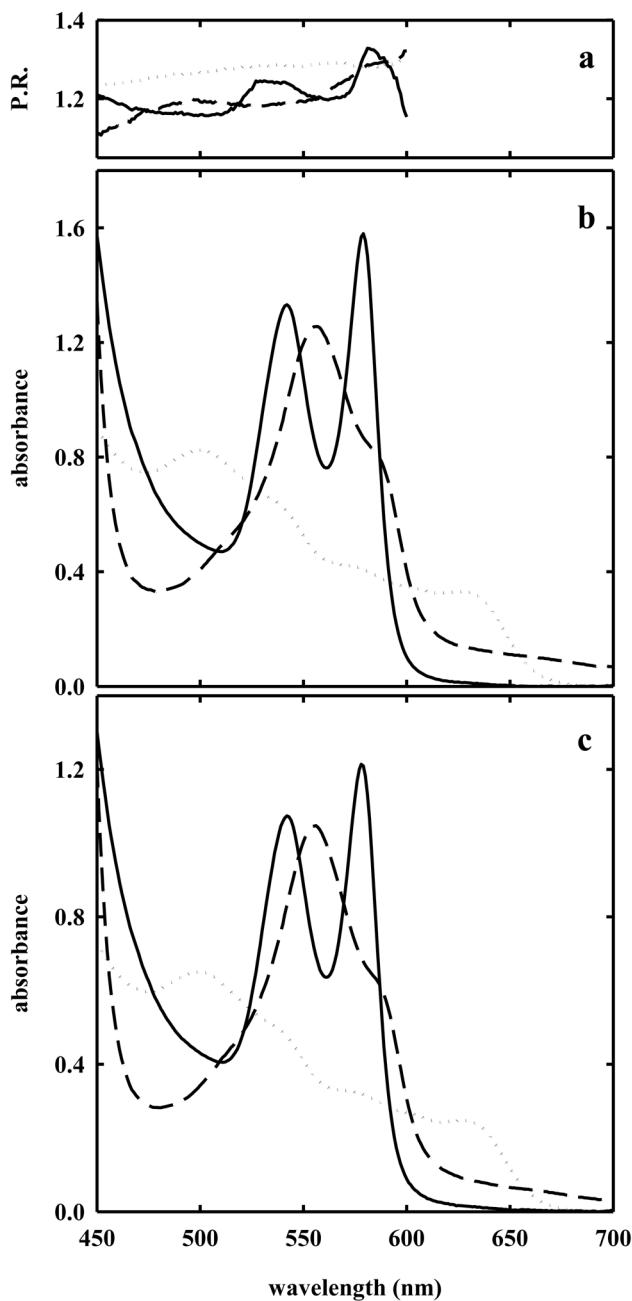and 5.6 µM HbII (dashed grey line), carried out at 20 °C in 100 mM phosphate, 1 mM
EDTA, pH 7.0.

Figure 7.
Polarized absorption spectra of HbII crystals soaked in 62% Na^+/K^+ phosphate, pH 7, 15 °C, collected with the electric vector of the polarized incident light parallel to the *c* (b) and *a* (c) crystal axis for oxy- (solid lines), deoxy- (dashed lines) and met- (dotted lines) species. The calculated polarization ratio is reported in (a).
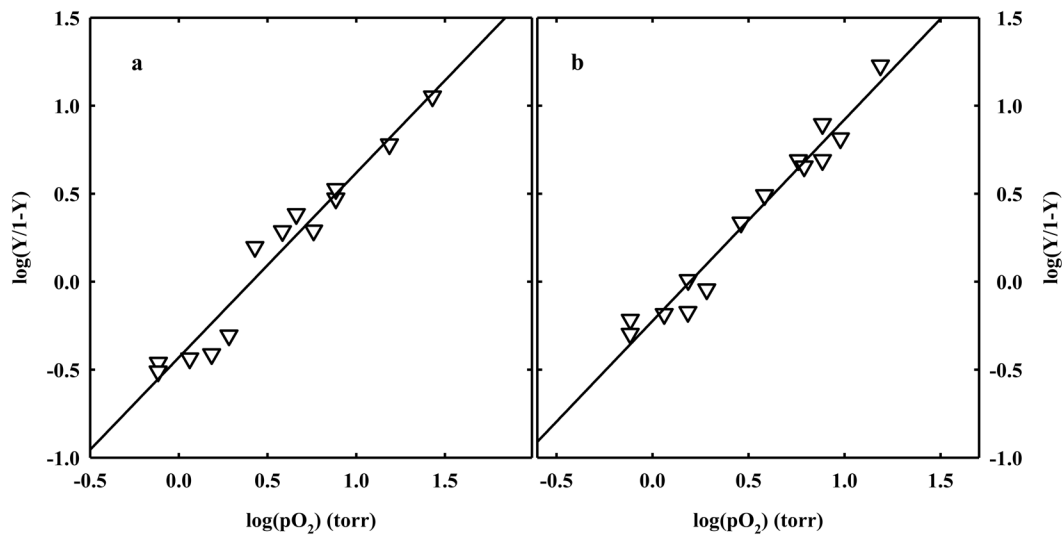
Figure 8.
Hill plots derived from oxygen binding curves recorded along the *c* (a) and *a* (b) crystal axis for HbII crystals soaked in 62% Na^+/K^+ phosphate, pH 7, at 15 °C. The calculated p50s are 2.57 ± 0.18 and 1.57 ± 0.10 torr, respectively, and the Hill coefficients are 1.05 ± 0.07 and 1.14 ± 0.06, respectively.
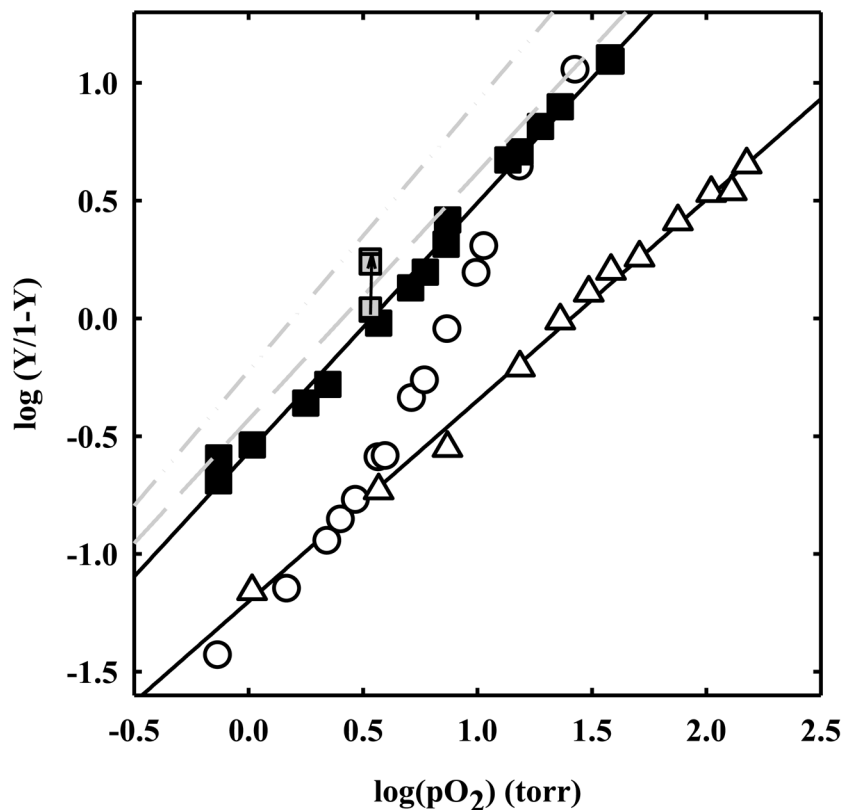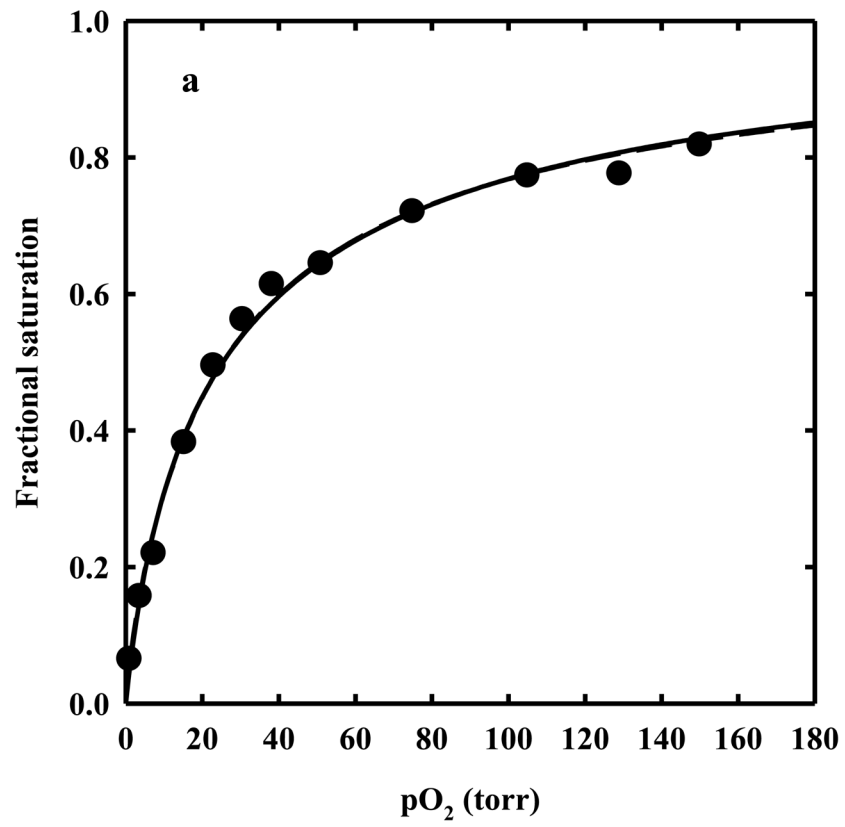
Figure 9.
Hill plots from oxygen binding curves to HbII in solution (open circles), or encapsulated in silica gel in T (open triangles up) and R state (closed squares). Fitting of the data points for T and R-state gels yields p50s of 25.6 ± 0.9 and 3.4 ± 0.1 torr with Hill coefficients of 0.85 ± 0.02 and 1.06 ± 0.02, respectively. For R state gels, fractional saturations at an oxygen pressure of 3.40 torr at increasing concentrations of phosphate from 100 to 400 and 600 mM are also reported (grey squares). Hill plots for HbII crystals oxygen binding curves measured along the *c* (dashed line) and *a* (dash-dot-dotted line) extinction directions are reported as grey lines (data from figure 7).

Figure 10.
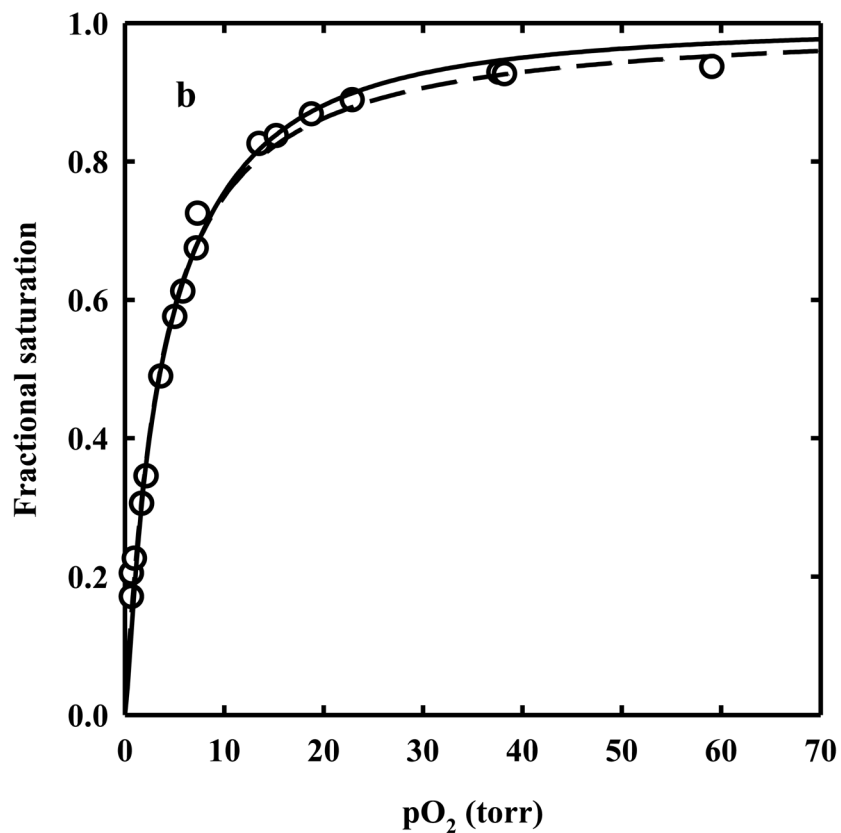a. T-state gel data (closed circles) fitted to the Hill equation (dashed line) and assuming two equally populated binding sites with no cooperativity (n=1) (solid line). The two curves are indistinguishable. b. R-state gel data (open circles) fitted to the Hill equation (dashed line) and assuming two equally populated binding sites with n=1.44 and an A/B inequivalence of 4.9 (solid line).

Table 1

Crystallographic statistics.

	HbII-CO	Unliganded HbII
Data collection		
Space group	$P2_12_12_1$	$P222_1$
Cell dimensions		
a, b, c (Å)	92.54, 99.88, 125.24	94.35, 100.96, 127.17
Resolution (Å)	50–1.24 (1.29–1.24)	50–1.45 (1.5–1.45)
R_{sym} (%)	5.9 (38.1)	6.7 (28.5)
$I/\sigma I$	29.5 (3.3)	13.9 (2.7)
Completeness (%)	98.9 (98.1)	92.2 (90.0)
Redundancy	6.2 (4.5)	3.5 (3.2)
Refinement		
Resolution (Å)	30.0–1.25	30–1.45
No. reflections	271,903	187,067
No. reflection test set	14,225	9,800
R_{work}/R_{free} (%)	13.7/17.4	13.3/17.5
No. atoms		
Protein	9,626	9,361
Heme	344	344
CO ligand	16	0
Water	1,984	1,945
Phosphate ion	0	4
No. residues with alternate conformations	86	47
B-factors (Å^2)		
Protein	15.1	12.6
Heme	13.9	10.4
CO ligand	14.1	-
Water	30.4	28.3
Phosphate	-	32.6
r.m.s. deviations		
Bond lengths (Å)	0.009	0.009
Bond angles (°)	1.42	1.28
Ramachandran Plot		
Most favored (%)	96.3	96.2
Additionally allowed (%)	3.7	3.8
Generously allowed (%)	0.0	0.0
Disallowed (%)	0.0	0.0
Protein Data Bank ID code	4HRR	4HRT

Values in parentheses are for highest-resolution shell.

Table 2

Projections of heme planes in R state HbII crystals.

Subunit[a]	$\sin^2 z_i a$[b]	$\sin^2 z_i b$[b]	$\sin^2 z_i c$[b]
	deoxyHbII		
A	0.0300	0.9808	0.9892
B	0.5028	0.9362	0.5611
C	0.9865	0.8240	0.1895
D	0.4941	0.6290	0.8769
E	0.9973	0.8237	0.1790
F	0.5463	0.6164	0.8373
G	0.0167	0.9841	0.9993
H	0.5762	0.9443	0.4794
	HbII CO		
A	0.9770	0.7795	0.2435
B	0.4858	0.6256	0.8886
C	0.0443	0.9845	0.9712
D	0.5684	0.9612	0.4704
E	0.9860	0.8108	0.2031
F	0.4467	0.6555	0.8978
G	0.0496	0.9765	0.9739
H	0.6079	0.9496	0.4425

[a] Subunits A, C, E and G are "A" chains and subunits B, D, F and H are "B" chains.

[b] $z_i a$, $z_i b$ and $z_i c$ are the angles between the normal to the plane of the heme cromophore (taken as the z molecular axis) and the a, b and c crystal axes. The plane of each heme cromophore was calculated using the 24 heme ring atoms (carbons and nitrogens). All normal vectors are chosen for simplicity so that the first component is positive; each normal vector is just the normalized eigenvector corresponding to the smallest eigenvalue of the moment-of-inertia tensor for that heme.

The fractional projections of the A hemes onto the a and c crystal axes, and therefore their fractional contribution to absorption measured along the two axes, are 0.489 and 0.461 for deoxyHbII, and 0.494 and 0.470 for HbII CO, respectively.